31st Congress of the International Council of the Aeronautical Sciences

Belo Horizonte, Brazil; September 09-14, 2018

ON WAKE VORTEX SAFETY ANALYSIS AND CONTROL FOR UAV

Vladimir Golubev* , **Petr Kazarin*** , **Claudia Moreno*** , **William MacKunis***
***Embry-Riddle Aeronautical University**

Keywords: *wake vortex, nonlinear,robust,control, modeling*

Abstract

External disturbances, such as turbulence wind gusts and upstream wake vortex can significantly affect the dynamics and flight trajectory of an unmanned aerial vehicle (UAV) . These effects can pose danger to UAV. Thus, the integration of Unmanned Aerial Systems (UAS) into National Airspace System (NAS) requires close consideration of these effects. This paper presents a robust nonlinear control method that can be proven to achieve altitude and roll regulation in the presence of several types of disturbances such as wake vortex and wind gust disturbance. Side-by-side simulation comparisons with H_∞ linear control method are provided. The results demonstrate the capability of the proposed nonlinear controller to asymptotically reject disturbances in the presence of parametric uncertainty. In addition, the nonlinear controller is designed with a computationally simplistic structure, which does not require complex calculations or function approximators in the control loop. Hence, the proposed controller is a great choice for small UAV applications with limited computational resources.

1 Introduction

The Federal Aviation Administration (FAA) currently addresses a number of safety challenges that exist in integrating UAS in the NAS. In order to improve the safety of UAS operating in the NAS, it is important to develop the novel UAV flight control technologies. Specifically, there is a need for control system technologies that are capable of quickly recovering from unpredictable and potentially hazardous operating conditions resulting from phenomena such as airflow disturbances created by upstream wake vortex, wind gusts, or turbulence. Based on these considerations, the focus of the current work is on the development of a nonlinear control method that demonstrates reliable and accurate UAV trajectory regulation in the presence of unmodeled and time-varying operating conditions in addition to uncertainty in the governing UAS dynamic model.
In this paper, a robust nonlinear flight control strategy in the presence of the wind gust as well as the wake vortex disturbance is presented. The analysis of the robust nonlinear controller in comparison to a linear H_∞ controller for several cases is demonstrated. The current work is an extension of the previous papers [1,2].

2 Mathematical Model

This section describes the mathematical model utilized to develop our nonlinear control method. The subsequently provided numerical simulation results were obtained using the mathematical models presented in this section for the UAV and wind gusts. The UAV dynamic model under consideration in this paper is assumed to contain parametric model uncertainty in addition to unmodeled, time-varying nonlinearities. The aircraft dynamics can be modeled via a quasi-linear

state space system as [3–5]

$$\begin{aligned} \dot{x} &= A(\rho)x + B(\rho)u + f(x,t) \\ y &= C(\rho)x + D(\rho)u \end{aligned} \tag{1}$$

where ρ is a measurable exogenous parameter vector, called the scheduling parameter, $x \in R^n$ are the deviation states, $u \in R^m$ are the deviation inputs, $y \in R^p$ are the deviation outputs, and $f(x,t)$ is an unknown nonlinear disturbance. Here, $A(\rho) \in R^{n\times n}$ represents the system matrix, $B(\rho) \in R^{n\times m}$ the input matrix, $C(\rho) \in R^{p\times n}$ the output matrix, and $D(\rho) \in R^{p\times m}$ the feedthrough matrix. The system is then arranged such that

$$A(\rho) = A_0 + \sum_{i=1}^{k} \delta_i A_i \tag{2}$$

$$B(\rho) = B_0 + \sum_{i=1}^{k} \delta_i B_i \tag{3}$$

$$C(\rho) = C_0 + \sum_{i=1}^{k} \delta_i C_i \tag{4}$$

$$D(\rho) = D_0 + \sum_{i=1}^{k} \delta_i D_i \tag{5}$$

where A_0, B_0, C_0, and D_0 are the nominal state space matrices. The parametric uncertainty is reflected by $\delta_i \in [-1,1]$, and the structural knowledge about the uncertainty is contained in the matrices A_i, B_i, C_i, and D_i [6]. This paper will be focused on the longitudinal and lateral control of a small UAV.

The longitudinal dynamics of an aircraft is described by the state vector $x = [u,w,q,\theta,Z_e]^T$, input vector $u = [\delta_e,\delta_\tau]^T$, and output vector $y = [V,\alpha,q,\theta,h,a_x,a_z]^T$. Here, u is the axial velocity, w is the vertical velocity, q is the pitch rate, θ is the pitch angle, and Z_e is the vertical position of the aircraft with respect to the horizon. In addition, δ_e is the elevator deflection, δ_τ is the throttle input, V is the true airspeed, α is the angle of attack, h is the altitude, a_x is the axial acceleration, a_z is the vertical acceleration. The scheduling parameter ρ can be altitude and Mach number and the unknown disturbance $f(x,t)$ could be wind gusts or nonlinearities not captured in the linear model.

The state vector for lateral dynamics is $x = [v,p,r,\phi,\psi]^T$ with input vector $u = [\delta_a,\delta_r]^T$. Where v,p,r,ϕ,ψ is lateral velocity, roll and yaw rates and angles. The input parameters are aileron and rudder deflections.

3 Numerical Simulation

3.1 Linear, Parameter-Varying Model

For further comparison of linear vs nonlinear control designs, the current paper will use a linear, parameter-varying (LPV) model based on a small fixed-wing UAV. The UAV selected for numerical simulations is the Ultrastick 120 for which the aerodynamics and flight dynamics has been widely studied [7, 8]. Figure 1 shows a picture of the UAV airframe. The LPV model is created by linearizing the nonlinear equations of motion about a set of equilibrium points. Here, the LPV model of the Ultrastick 120 holds a constant altitude and varying airspeed.

Fig. 1 Ultra Stick 120. Source: UAV Laboratories, University of Minnesota

The Ultrastick 120 LPV model is then generated by obtaining a set of equilibrium points holding a constant altitude of 100 m and varying airspeed between 15-29 m/s. These equilibrium points are shown in Figure 2 where airspeed $V = 23$ m/s is chosen as the nominal flight condition. Robust nonlinear and linear controllers for such UAV designed, with performance analysis presented below.

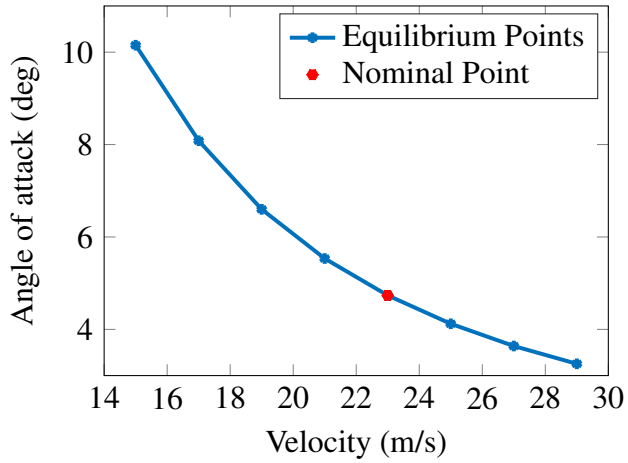

Fig. 2 Varying parameter trajectory: set of equilibrium points for LPV model

3.2 H_∞ Linear Controller

The details of H_∞ controller design can be found in the previous paper [2].

4 Nonlinear Robust Control

4.1 Control Objective

The control objective is divided into two parts: one for longitudinal dynamics and one for the lateral dynamics. The goal is to force the UAV altitude and pitch rate (i.e., $h(t)$ and $q(t)$) to track a given desired constant value (longitudinal) as well as roll and yaw rates (i.e., r and p))(lateral) in spite of model uncertainty and external disturbances.

To quantify the control objective, the trajectory regulation error $e(t) \in R^2$ and auxiliary regulation error $r(t)$ $\begin{bmatrix} r_q(t) & r_h(t) \end{bmatrix}^T \in R^2$ are defined as

$$e(t) = \begin{bmatrix} h(t) \\ \theta(t) \end{bmatrix} \tag{6}$$

$$r(t) = \begin{bmatrix} r_h(t) \\ r_q(t) \end{bmatrix} = \begin{bmatrix} \dot{h}(t) + \alpha_1 h(t) \\ q(t) + \alpha_2 \theta(t) \end{bmatrix} \tag{7}$$

In case of lateral motion, the auxiliary regulation error $r(t)$ $\begin{bmatrix} r_p(t) & r_r(t) \end{bmatrix}^T \in R^2$ and roll/yaw regulation error are as follows:

$$e(t) = \begin{bmatrix} \phi(t) \\ \psi(t) \end{bmatrix} \tag{8}$$

$$r(t) = \begin{bmatrix} r_p(t) \\ r_r(t) \end{bmatrix} = \begin{bmatrix} \dot{\phi}(t) + \alpha_1 \phi(t) \\ \dot{\psi}(t) + \alpha_2 \psi(t) \end{bmatrix} \tag{9}$$

In equations (7,9) $\alpha_1, \alpha_2 \in R$ denote positive, constant control gains.

Thus, the trajectory regulation control objective can be stated mathematically as $\|e(t)\| \to 0$, where $\|a\|$ denotes the standard Euclidean norm of the vector argument. Note that, based on the auxiliary regulation error definitions in equations (7,9), $\|r(t)\| \to 0 \Rightarrow \|e(t)\| \to 0$.

Remark 1: The regulation error and auxiliary errors defined in Equations (6,8) and (7,9) are a key aspect of the contribution presented here. The definitions of the auxiliary regulation errors enable us to recast the dynamic model in Equation (1) in a form that is amenable to altitude/pitch angle and roll/yaw angle regulation control. Indeed, it can be seen that differentiation of $r(t)$ produces a set of equations that render the altitude and pitch angle states ($h(t)$ and $\theta(t)$) and roll/yaw angles (ϕ, ψ) fully controllable through the elevator deflection and throttle inputs $\delta_e(t)$, $\delta_t(t)$ and $\delta_a(t)$, $\delta_r(t)$. Thus, the auxiliary error terms $r_h(t)$,$r_q(t)$, $r_r(t)$,$r_p(t)$ can be viewed as sliding surfaces, which enables us to prove our altitude and pitch angle regulation results.

4.2 Robust Controller Development

In order to achieve asymptotic convergence of θ, h and ϕ, ψ to zero with a given convergence rate in the presence of a bounded disturbance (i.e. wake vortex or wind gust), we have to drive the auxiliary regulation error r to zero in finite time.

Taking into account the original dynamic model, and the auxiliary regulation error r, the auxiliary control term u is designed as:

$$\begin{bmatrix} u \end{bmatrix} = \begin{bmatrix} \hat{\Omega}^{-1} \end{bmatrix} \begin{bmatrix} k_1 r_{h,r} \\ k_2 r_{q,p} \end{bmatrix} + \begin{bmatrix} \beta_1 tanh(r_{h,r}) \\ \beta_2 tanh(r_{q,p}) \end{bmatrix} \tag{10}$$

where $\hat{\Omega}$ denotes a constant auxiliary matrix, and $[]^{-1}$ denotes the inverse of a matrix. The feedback control gains (i.e., amplifiers)

k_1,k_2,β_1,β_2 can be tuned to adjust the closed loop regulation response to achieve the desired system performance (e.g., to achieve a faster response time).

Note that the continuous $tanh()$ switching term in Equation 10 is used in the subsequent simulation implementation, but the discontinuous $signum()$ function is required to prove asymptotic disturbance rejection as shown in reference [2] .

The feedback control gains (i.e., amplifiers) $\alpha_1, \alpha_2, \beta_1, \beta_2, k_1, k_2$ can be tuned to adjust the closed loop trajectory regulation response to achieve the desired system performance (e.g., to achieve a faster response time).

4.3 Wind Gust Model

The performance of the nonlinear robust controller is tested using the Matlab/Simulink software. The simulation is based on state space systems describing each particular equilibrium point of LPV model described above.

Similar to [1] the aircraft longitudinal performance is evaluated for a nonlinear disturbance in the form of a vertical wind gust described as[9],

$$f(x,t) = w_g \frac{1}{V_0} \left\{ \frac{U_{ds}}{2} \left[1 - cos\left(\frac{\pi s}{H} \right) \right] \right\} \quad (11)$$

where H denotes the distance (between 35 feet and 350 feet) along the aircraft flight path for the gust to reach its peak velocity, V_0 is the forward velocity of the aircraft when it enters the gust, $s \in [0, 2H]$ represents the distance penetrated into the gust (i.e., $s = \int_{t_1}^{t_2} V(t)dt$, where $V(t)$ is the forward velocity element of the state vector x), and U_{ds} is the design gust velocity[9]. The vector $w_g \in R^5$ represents the relative impact of the gust on each state of the system. This FAR formulation is intended to be used to evaluate both vertical and lateral gust loads, so a similar representation can be developed for the lateral dynamics. This simulation uses the parameters $H = 15.24m$, and V_0 equal to the speed in current trim state, (cruise velocity). Since the state vector is this case is defined as $x(t)\,[v(t) \quad w(t) \quad q(t) \quad \theta(t) \quad h(t)]$, the constant gain parameters of simulated model were modified slightly from (11). The remainder of the additive disturbances in $f(x,t)$ represents nonlinearities not captured in the linearized state space model (e.g., due to small angle assumptions).

4.4 Wake vortex Model

The aircraft lateral performance is evaluated for a nonlinear disturbance in the form of vortex-induced flow field modeled with the Burnham-Hallock Vortex Model[10].

$$V_\theta = \frac{\Gamma_0}{2\pi r} \frac{r^2}{r^2 + {r_c}^2} \quad (12)$$

The wake vortex is supposed to be generated by the leader aircraft with elliptical load on the wings. It is presented by two counter-rotating vortex flow fields which are superimposed resulting in cumulative load on the follower aircraft.

After the calculation of the induced angle of attack at each point of the aircraft's wing, the strip theory is further applied to calculate the induced roll moment coefficient and induced lift.

When considering the aircraft response, the roll moment dependence on aircraft roll angle results in nonlinear coupling.

Wake vortex decay is described by two-phase low fidelity model from our previous study[11]. The time history of the wake vortex circulation decay behind the leader aircraft (B-733) is shown in Figure 10. This is the case from data set of LIDAR measurements obtained at Denver International Airport in 2003 [12]. The ambient turbulence level as well as the atmospheric stratification profile was taken into account when simulating the vortex decay.

5 Results

This section first presents the results of our previous study[2], where the analysis of the robust nonlinear controller performance in comparison with the linear H_∞ controller performance described above and also in Dorbantu et al[13], with the same performance objectives, is shown. The

aim of the regulation is to drive the altitude and pitch rate deviations to zero.

Figures 4, 5 show the detailed time evolution of the flight trajectories during closed-loop linear and nonlinear controller operation for two trim conditions (23 m/s and 21 m/s) and equal gust amplitudes of 17 m/s. The pitch rate and pitch angle deviations for 21 m/s equilibrium point are lower in case of nonlinear controller. However the altitude deviation is slightly lower for linear control law. For the nominal trim point, the altitude deviation remains almost the same for the two controllers, but the pitch rate and pitch angle disturbances turn out to be much lower for the nonlinear controller. For the nominal equilibrium point, nonlinear controller significantly outperforms the linear one in terms of the elevator deflection, however throttle power required by the linear controller is much lower. When the trim condition changes from nominal, the nonlinear controller still works better in terms of pitch rate and pitch angle deviations. The control power for elevator input is still small for the nonlinear case and the throttle inputs are almost the same. More detailed consideration of the wind gust impact can be found in [2].

We now consider the follower aircraft response to the wake vortex induced disturbance. Two time moments (130 s and 155 s) with circulations of $\Gamma = 16m^2/s$ and $\Gamma = 32m^2/s$ are examined. This corresponds to the distance of 4.6 NM and distance is 5.5 NM from the leader aircraft since it has the speed of 65 m/s (Figure 10). The follower airplane is placed 5 m lower in altitude relative to the leader aircraft in both cases considered. The results of the applied controls indicate that the Ultrastick-120 is able to reject the disturbance effect of the separation distance of 5.5 nautical miles (NM) but fails to implement the control objective for 4.6 NM. The results are illustrated in Figures 6,11,12,8 and 7,13,14,9. In this two cases Ultrastick 120 is following B-733. The Ultrastick's 120 response to the wake vortex induced disturbance is modeled by changing its horizontal position or "dragging" the airplane through the wake in the plane of the leader aircraft. Several positions of the follower airplane are shown in Figure 3.

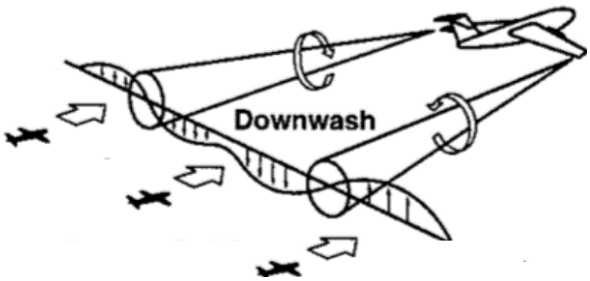

Fig. 3 Schematic view of the wake-vortex generating leader aircraft and several positions of the follower aircraft [14]

Longitudinal and lateral responses are considered separately. The lateral response is presented in Figure 6. The lateral disturbance affects both the roll and horizontal speed of the airplane (Figure 11). One can see that the roll disturbance changes the sign depending on the position of the airplane. The corresponding deflections of the right and left ailerons as well as the rudder are shown in Figure 12. As discussed above, wake vortex also creates the wake vortex induced lift on the wing, which results in the vertical disturbance. In this case, the longitudinal nonlinear controller successfully controls the impact.

However, due to the rate and deflection limits of the control surfaces (150 deg/s and 25 deg), the nonlinear controller fails to control the wake impact when the separation distance is too short. As shown in Figure14, there is not enough power created by the rudder to have enough control authority. As a result, the horizontal aircraft velocity is divergent (Figure 9).

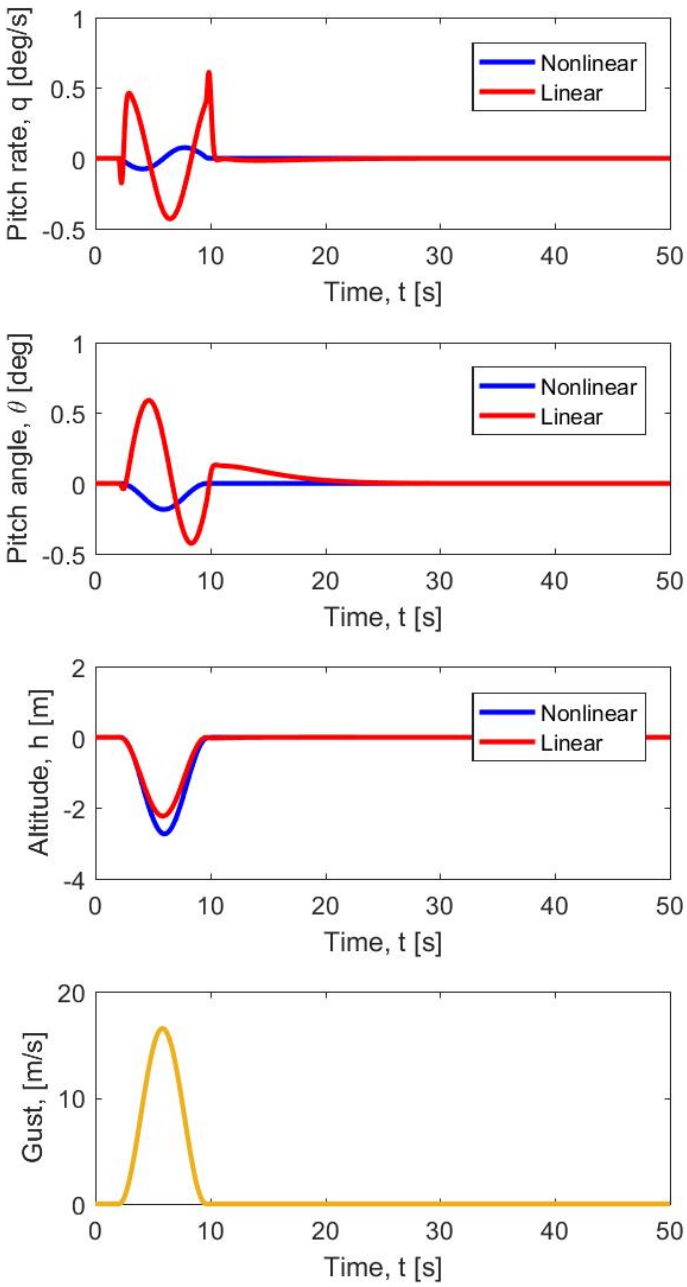

Fig. 4 Deviations of state variables for the nominal trim condition (23 m/s equilibrium point), 17 m/s gust

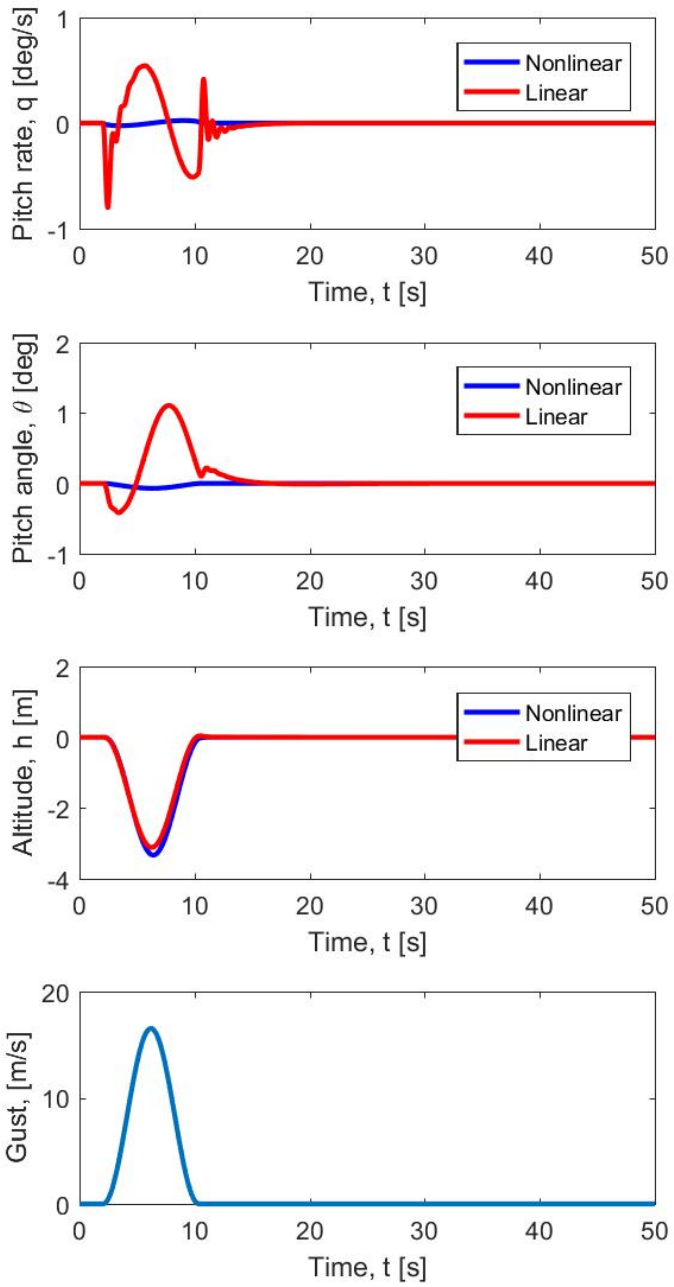

Fig. 5 Deviations of state variables for 21 m/s equilibrium point, 17 m/s gust

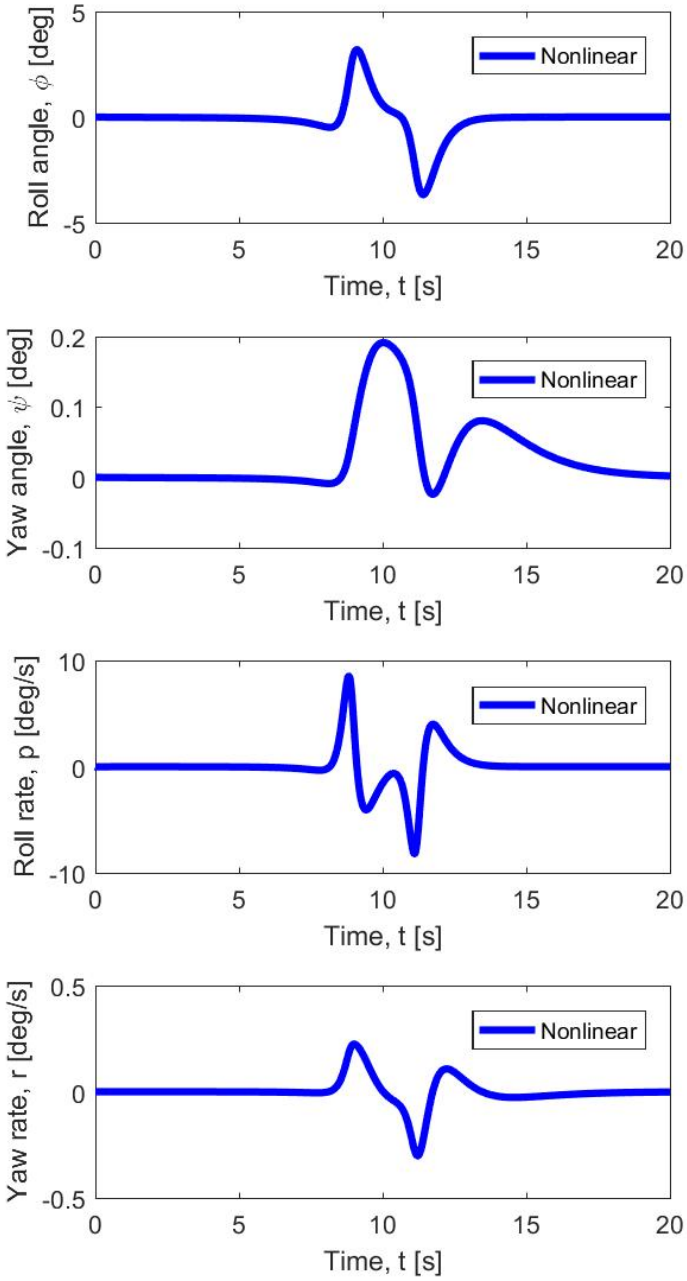

Fig. 6 Lateral states disturbed with wake vortex (the aircraft separation distance is 5.5 NM)

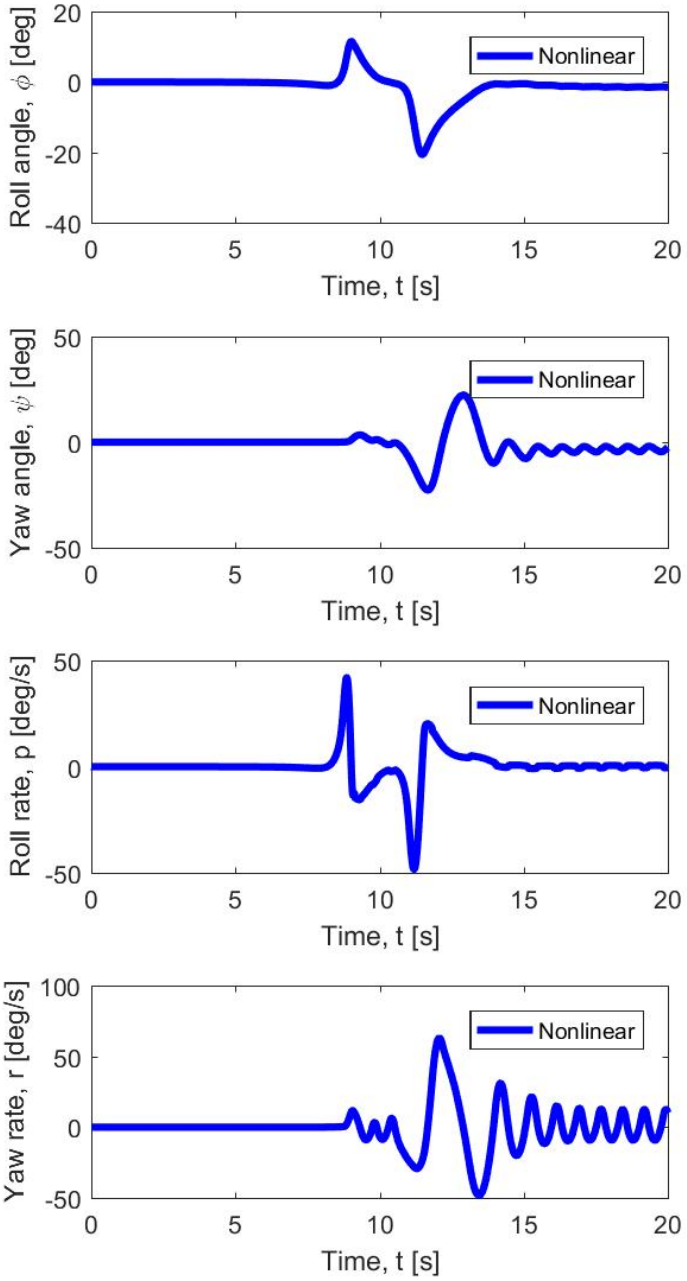

Fig. 7 Lateral states disturbed with wake vortex (the aircraft separation distance is 4.6 NM)

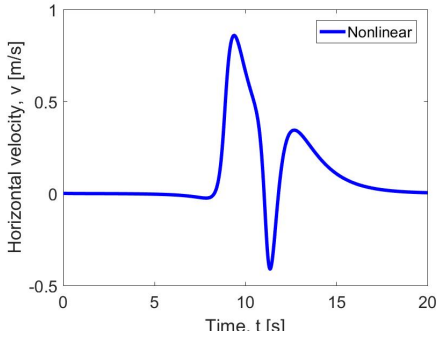

Fig. 8 Horizontal speed (the aircraft separation distance is 5.5 NM)

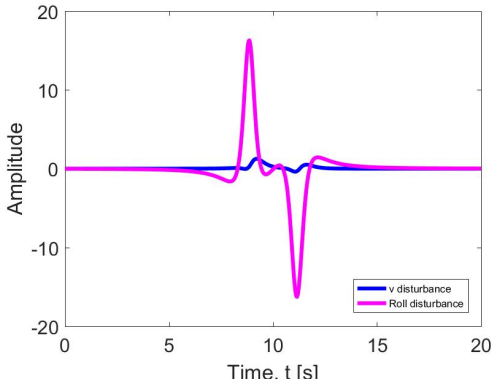

Fig. 11 Lateral disturbance from wake vortex (the aircraft separation distance is 5.5 NM)

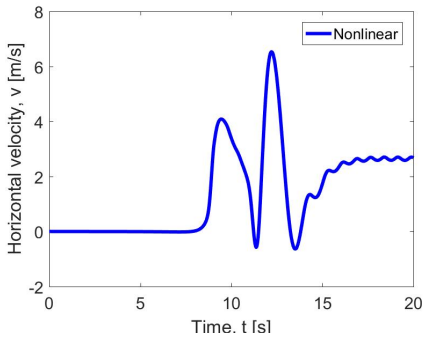

Fig. 9 Horizontal speed (the aircraft separation distance is 4.6 NM)

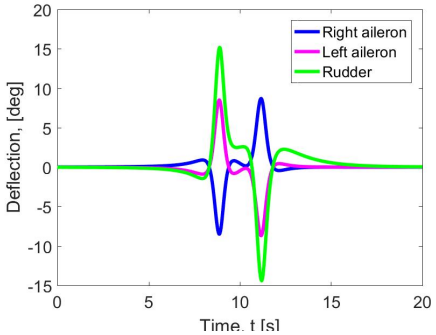

Fig. 12 Control surfaces deflection (ailerons and rudder) (the aircraft separation distance is 5.5 NM)

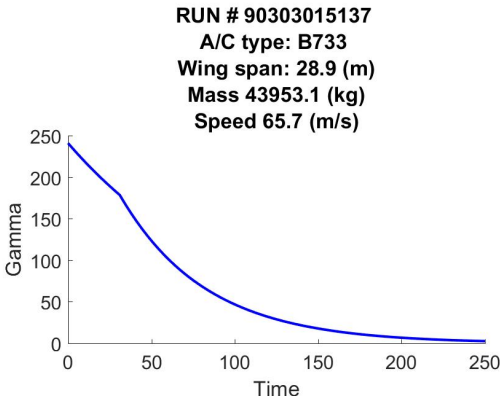

Fig. 10 Vortex Strength Decay Time History (B-733)

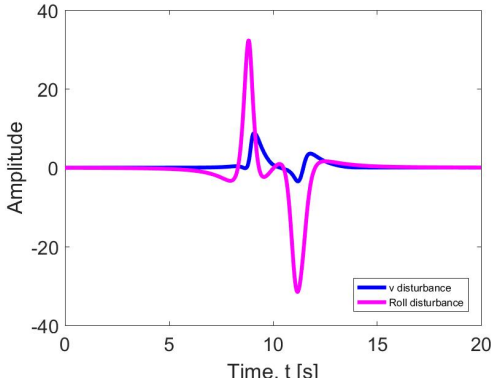

Fig. 13 Lateral disturbance from wake vortex (the aircraft separation distance is 4.6 NM)

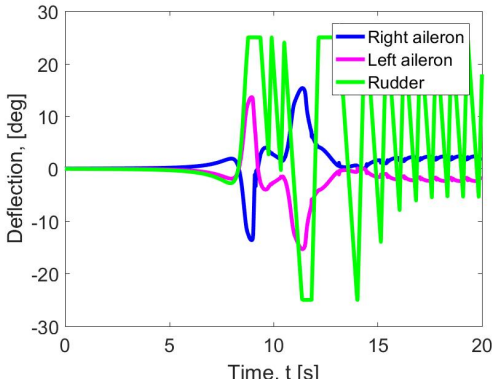

Fig. 14 Control surfaces deflection (ailerons and rudder) (the aircraft separation distance is 4.6 NM)

6 Conclusion

A nonlinear UAV regulation control method was presented, which can be proven to asymptotically regulate pitch angle and altitude in the presence of extreme wind gust disturbances and wake vortex disturbance. Detailed numerical simulation results were provided to demonstrate the performance of the proposed nonlinear control law. To provide a basis for comparison, the same control objective is simulated using a linear control law (gust case). It is shown that the nonlinear control method compensates for the wind gust disturbances significantly more effectively than the linear controller. Moreover, parameter variations in the state space model were introduced in the simulation. Both nonlinear and linear controllers were tested in the presence of uncertainty in the aircraft and an actuator's dynamic model.The results showed that the nonlinear control design outperformed the linear control method for the simulated trajectory regulation objective under the tested levels of uncertainty. In the current work, the performance of the nonlinear controller is successfully tested in the presence of the wake vortex disturbance created by the leader aircraft (B-733). In the future work, the performance of H_∞ linear controller in the presence of the wake vortex gust will be demonstrated and compared to the nonlinear robust controller performance.

References

[1] Golubev, V, Kazarin, P, MacKunis, W, Borener, S, and Hufty, D. *On safety assessment of novel approach to robust UAV flight control in gusty environments*. ICAS 2016.

[2] Kazarin, P, MacKunis, WT, Moreno, CP, and Golubev, VV. *Robust nonlinear tracking control for unmanned aircraft with synthetic jet actuators*. In: *AIAA Atmospheric Flight Mechanics Conference*. 2017.

[3] Deb, D, Tao, G, Burkholder, JO, and Smith, DR. *Adaptive compensation control of synthetic jet actuator arrays for airfoil virtual shaping*. Journal of aircraft 2007;44.

[4] Deb, D, Tao, G, Burkholder, JO, and Smith, DR. *Adaptive synthetic jet actuator compensation for a nonlinear aircraft model at low angles of attack*. IEEE Transactions on Control Systems Technology 2008;Vol.16.

[5] Mondschein, ST, Tao, G, and Burkholder, JO. *Adaptive actuator nonlinearity compensation and disturbance rejection with an aircraft application*. In: *Proceedings of the 2011 American Control Conference*. IEEE. 2011.

[6] Zhou, K, Doyle, J, and Glover, K. *Robust and optimal control*. Prentice Hall, 1995.

[7] Freeman, PM. *Reliability assessment for low-cost unmanned aerial vehicles*. PhD thesis. University of Minnesota, 2014.

[8] Dorobantu, A, Murch, A, Mettler, B, and Balas, G. *Frequency domain system identification for a small, low-cost, fixed-wing UAV*. In: *AIAA Guidance, Navigation, and Control Conference*. 2011.

[9] Part, FAR. *25: Airworthiness standards: Transport category airplanes*. Federal Aviation Administration, Washington, DC 2002;Vol.7.

[10] Burnham, D and Hallock, JN. *Chicago monostatic scoustic vortex sensing system. volume IV. Wake vortex decay.* Tech. rep. Transportation systems Center Cambridge MA, 1982.

[11] Kazarin, P, Provalov, A, and Golubev, VV. *Comparison of probabilistic approaches for predicting the cone of uncertainty in aircraft wake vortex evolution*. In: *9th AIAA Atmospheric and Space Environments Conference*. 2017.

[12] Gloudemans, T, Van Lochem, S, Ras, E, Malissa, J, Ahmad, NN, and Lewis, TA. *A coupled probabilistic wake vortex and aircraft response prediction model*. NASA Technical Report 2016.

[13] Dorobantu, A, Murch, A, Mettler, B, and Balas, G. *System identification for small, low-cost, fixed-wing unmanned aircraft*. Journal of Aircraft 2013;Vol.50.

[14] Barbeau, Z and Jacob, JD. *Experimental flight test of small UAS wake vortex encounters*. In: *55th AIAA Aerospace Sciences Meeting*. 2017.

7 Contact Author Email Address

Vladimir Golubev, mailto: golubd1b@erau.edu

Copyright Statement